NASA TECHNICAL NOTE

NASA TN D-3763

NASA TN D-3763

ANALYSIS OF SOLIDIFICATION IN THERMAL-ENERGY STORAGE SYSTEMS WITH AXISYMMETRIC HEAT-TRANSFER SOLUTIONS

by Richard R. Cullom, George Diedrich, and Lynn U. Albers

Lewis Research Center

Cleveland, Ohio

NATIONAL AERONAUTICS AND SPACE ADMINISTRATION • WASHINGTON, D. C. • DECEMBER 1966

NASA TN D-3763

ANALYSIS OF SOLIDIFICATION IN THERMAL-ENERGY STORAGE SYSTEMS WITH AXISYMMETRIC HEAT-TRANSFER SOLUTIONS

By Richard R. Cullom, George Diedrich, and Lynn U. Albers

Lewis Research Center
Cleveland, Ohio

NATIONAL AERONAUTICS AND SPACE ADMINISTRATION

For sale by the Clearinghouse for Federal Scientific and Technical Information
Springfield, Virginia 22151 – Price $1.00

ANALYSIS OF SOLIDIFICATION IN THERMAL-ENERGY STORAGE SYSTEMS WITH AXISYMMETRIC HEAT-TRANSFER SOLUTIONS

by Richard R. Cullom, George Diedrich, and Lynn U. Albers

Lewis Research Center

SUMMARY

An analysis was made of a transient heat conduction problem with a phase change in the axisymmetric conducting medium and heat transfer at the inner radius only. Nondimensional finite-difference solutions for surface temperature and solidification thickness were obtained for a range of time, initial heat-rejection rate, tube diameter, and storage-material properties. Although the configuration of a tube submerged in a thermal-energy storage material which is at its fusion temperature applies to space auxiliary-power systems, the nondimensional solutions presented in this report can be applied to a wide range of axisymmetric solidification problems, such as metal casting and ice formation.

To illustrate their application, the general solutions were used in an analysis of a lithium hydride thermal-energy storage system. Analysis indicates that the use of axisymmetric solutions are recommended over the simple one-dimensional solutions for low radii or long dark times to prevent inefficient overdesign of the thermal-energy storage component. The storage-material surface temperature is more sensitive to changes in heat-rejection rate than to changes in either cooling time or heat-transfer surface radius. The solidification thickness is a stronger function of cooling time than either heat-transfer rate or surface radius.

INTRODUCTION

The solar Rankine and Brayton cycle engines are being considered as possible power sources for space missions. Providing energy to the conversion device while the satellite is in the eclipsed, or dark portion of its orbit, is a problem common to these solar-energized orbiting auxiliary-power systems. A method of providing power for the duration of the orbital dark time is to store the solar thermal energy as the latent heat of fu-

sion of a suitable material. A component common to the solar thermal-energy storage systems is the cavity-absorber, which receives and transfers the incident radiant thermal flux into the conversion system. The cavity-absorber usually contains thermal-energy storage material between the cavity wall and the heat-transfer loop which conveys the absorbed thermal energy to the conversion system. In orbit this storage material is melted by solar radiation. It then supplies thermal energy, theoretically equal to its latent heat of fusion, to the energy-conversion system during periods when the solar collector is shadowed from the Sun. Thermal-energy storage is attractive in auxiliary systems because the relatively high specific storage capability minimizes the overall weight of the power system. In addition, the basic simplicity of the concept is expected to result in high reliability and long life.

Solutions to the transient heat-transfer process that occurs during the extraction of heat from a melted storage material will aid greatly in the design and estimation of performance of thermal-storage systems. Solutions for transient heat conduction for various boundary conditions with a change of phase of the one-dimensional conducting medium have been developed (refs. 1 to 3). These one-dimensional solutions can be applied to problems involving metal casting and ice formation and to axisymmetric storage systems in which solidification thickness is small relative to the tube diameter. To aid in the design and evaluation of a greater range of tube-type thermal-energy storage systems and to solve general axisymmetric solidification problems, this report presents the difference solutions for transient heat conduction with a phase change in the axisymmetric conducting medium. Nondimensional solutions for the surface temperature and solidification thickness of storage material were obtained for a range of time, initial heat-rejection rate, tube diameter, and storage-material properties. Although this study was motivated by the space application of thermal-energy storage, the solutions presented herein can be applied to many axisymmetric problems, such as metal casting and ice formation.

ANALYSIS

The thermal-energy storage model considered herein is an axisymmetric, time-variant, heat-conduction system with a change in state of the conducting medium (fig. 1). The thermal-storage material is assumed to be semi-infinite. The thermal energy supplied by the conversion of its latent heat of fusion at the solid-liquid interface causes the surrounding liquid to freeze. The thermal energy is then conducted through the solidified phase and convected to the heat-transfer fluid at the inner radius surface. The storage material properties are assumed to be invariant with temperature. With these assumptions, the transient heat-conduction equation is

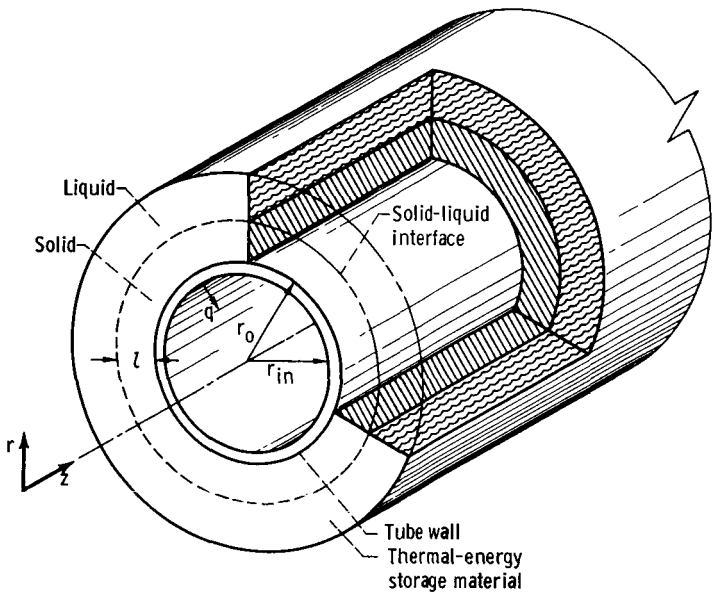

Figure 1. - Thermal-energy-storage model during heat-transfer process.

$$\frac{\partial T}{\partial t} = \alpha\left(\frac{\partial^2 T}{\partial r^2} + \frac{1}{r}\frac{\partial T}{\partial r}\right) \qquad \text{for} \quad r_o < r < r_o + l \tag{1}$$

(Symbols are defined in the appendix.) The boundary conditions for the thermal-storage model shown in figure 1 are established as follows. Initially, the complete volume of the heat-storage material is assumed to be in the liquid phase and at the fusion temperature:

$$\left.\begin{aligned} T &= T_f \\ l &= 0 \end{aligned}\right\} \text{at} \quad t = 0$$

As thermal energy is extracted from the storage material, the surface temperature drops below the fusion temperature, and the liquid phase is solidified. This phase is assumed to be stagnant but continually in intimate contact with the solid-liquid interface. The interface moves in the positive r-direction; at the interface the temperature is equal to the fusion temperature:

$$T = T_f \qquad \text{at} \quad r = r_o + l$$

In a heat balance at the solid-liquid interface, the rate at which the heat of fusion is liberated by the solidifying material is equal to the rate at which heat is transferred from the interface into the solidified phase:

$$\rho f \frac{dl}{dt} = k \frac{\partial T}{\partial r} \qquad \text{at} \quad r = r_o + l$$

A heat balance at the inner radius surface of the storage material equates the convective heat transfer to the fluid with the rate at which heat is conducted toward the surface of the solidified material:

$$h(T - T_b) = k \frac{\partial T}{\partial r} \qquad \text{at} \quad r = r_o$$

In this equation h is the overall heat-transfer coefficient and includes the tube-wall resistance as well as the surface resistance to heat transfer. However, when $t = 0$ and $T = T_f$, then $h(T_f - T_b)$ is defined as the initial heat-rejection rate.

Equation (1) may be nondimensionalized by expressing the variables in terms of the following dimensionless parameters:

$$\varphi = \frac{T - T_b}{T_f - T_b} \tag{2}$$

$$\tau = \frac{h^2 \alpha t}{k^2} \tag{3}$$

$$R = \frac{hr}{k} \tag{4}$$

$$F = \frac{f}{c_p(T_f - T_b)} \tag{5}$$

$$L = \frac{hl}{k} \tag{6}$$

The resulting form of the heat-condition equation is

$$\varphi_\tau = \varphi_{RR} + \frac{\varphi_R}{R} \tag{7}$$

Equation (7) involves the dependent temperature-related variable φ and the two independent variables, the time-related variable τ and the space-related variable R. The

subscripts denote partial differentiation. The equation is to be satisfied at all points (R, τ) interior to the region $R_0 < R < R_0 + L(\tau)$ and $\tau > 0$. The function $L(\tau)$ is related to the thickness of the solidified layer, which increases with time.

The boundary conditions are

$$\varphi(R, 0) = 1 \qquad \text{for} \quad R > R_0 \tag{8}$$

$$\varphi_R(R_0, \tau) = \varphi(R_0, \tau) \qquad \text{for} \quad \tau > 0 \tag{9}$$

$$\varphi\left[R_0 + L(\tau), \tau\right] = 1 \qquad \text{for} \quad \tau > 0 \tag{10}$$

$$\frac{dL(\tau)}{d\tau} = \frac{\varphi_R}{F} \tag{11}$$

The first boundary condition, equation (8), states that initially the storage material is uniformly at the temperature of fusion. The second boundary condition describes how heat is withdrawn through the interior surface of the solid layer to the heat-transfer fluid. The third condition shows that the solid-liquid interface is always at the fusion temperature. The fourth condition states that the rate of growth of the layer thickness L is directly proportional to the temperature gradient at the solid-liquid interface and inversely proportional to a parameter F, which is related to the heat of fusion.

Solution of Heat-Conduction Equation

The heat-conduction equations were solved by finite-difference methods for a variety of parameter pairs R_0 and F. Some cases were solved by an explicit method, but excessive computing times for cases with small values of R_0 made it worthwhile to convert to the Crank-Nicholson method (ref. 4), which is implicit. The methods are described in the next two sections.

Explicit method. - In the integration from τ to $\tau + \Delta\tau$, the space derivatives are calculated at the time τ. This leads to explicit equations for the new φ's of the following forms. The equation at all interior points is

$$\varphi(R, \tau + \Delta\tau) = A_1\varphi(R - \Delta R, \tau) + A_2\varphi(R, \tau) + A_3\varphi(R + \Delta R, \tau) \tag{12}$$

where

$$A_1 = \beta - \frac{\gamma}{R}$$

$$A_2 = 1 - 2\beta$$

$$A_3 = \beta + \frac{\gamma}{R}$$

$$\beta = \frac{\Delta\tau}{(\Delta R)^2}$$

$$\gamma = \frac{\Delta\tau}{2\,\Delta R}$$

and the equation at the $R = R_0$ boundary is

$$\varphi(R_0, \tau + \Delta\tau) = B_1\varphi(R_0 + \Delta R, \tau + \Delta\tau) + B_2\varphi(R_0 + 2\,\Delta R, \tau + \Delta\tau) \tag{13}$$

where

$$B_1 = \frac{4}{3 + 2\,\Delta R}$$

$$B_2 = \frac{-1}{3 + 2\,\Delta R}$$

The latter arises from using a three-point Lagrangian derivative in the second boundary condition (eq. (9)). The new L value and the new φ value at the position $R = R_0 + L(\tau)$ are determined iteratively by use of the finite-difference analog of the fourth boundary condition. It is well known that this explicit process is unstable if the coefficient A_2 in equation (12) is negative; that is, unless $\Delta\tau$ is chosen to be less than $(\Delta R)^2/2$, the so-called safe step size for τ. This instability makes the explicit method time consuming for cases with small interior radius.

To minimize the truncation error caused by the one-sided character of the τ derivative, the explicit method was modified in the following manner. If the k^{th} approximation to $\varphi(R, \tau + \Delta\tau)$ is denoted by $\varphi_k(R)$ and the R derivatives are calculated about $\tau + \Delta\tau/2$, the iteration equation is obtained as

$$\varphi_{k+1}(R) = D_1\varphi(R - \Delta R, \tau) + (1 - \beta)\varphi(R, \tau) + D_2\varphi(R + \Delta R, \tau)$$

$$+ D_1\varphi_k(R - \Delta R) - \beta\varphi_k(R) + D_2\varphi_k(R + \Delta R) \quad (14)$$

where

$$D_1 = \frac{A_1}{2}$$

$$D_2 = \frac{A_3}{2}$$

This modification was unsuccessful in allowing use of a larger time step which would reduce computing time. Therefore, the modified explicit method was employed only in starting the implicit solutions, that is, until the growth of $L(\tau)$ began. However, certain test cases were completely integrated by using the modified explicit method.

Implicit method. - In the Crank-Nicolson method (ref. 4), the R derivative as well as the τ derivative is calculated about $\tau + \Delta\tau/2$. This leads to the basic implicit equation

$$-D_1\varphi(R - \Delta R, \tau + \Delta\tau) + (1 + \beta)\varphi(R, \tau + \Delta\tau) - D_2\varphi(R + \Delta R, \tau + \Delta\tau)$$

$$= D_1\varphi(R - \Delta R, \tau) + (1 - \beta)\varphi(R, \tau) + D_2\varphi(R + \Delta R, \tau) \quad (15)$$

This equation, together with the consequent of the second boundary condition,

$$(1 + \Delta R)\varphi(R_o, \tau + \Delta\tau) - \varphi(R_o + \Delta R, \tau + \Delta\tau) = 0 \quad (16)$$

reduces the integration process from τ to $\tau/\Delta\tau$ to the solution of a single matrix equation with a tridiagonal coefficient matrix. The matrix is factored into triangular factors, and the solution is carried out by the usual forward and backward substitution processes. No iteration is involved.

Because the coefficient $1 + \beta$ in equation (15) is positive for all steps in $\Delta\tau$, the Crank-Nicolson method is known to be stable. When results were compared to those obtained for the slower explicit method, it was found that a $\Delta\tau$ of 20 times the safe step was usable with no appreciable degradation in accuracy. Even allowing for the greater complexity of the implicit process, an overall speed gain of 10 to 1 was achieved.

Program Running Procedures

Input data cards were used to specify the two parameters, dimensionless radius R_o, which ranged from 0.01 to 100, and dimensionless heat of fusion F, which ranged from 0.1 to 25, as well as the starting thickness L. In general, L(0) was chosen as the smaller of the two numbers, either 0.001 R_o or 0.001, and ΔR was always L/20. Values of dimensionless temperature $\varphi(R_o, \tau)$ and solidification thickness $L(\tau)$ were obtained at dimensionless time steps of 0.1 for $\log_{10}\tau$ from -4.0 to 3.0. At the completion of each specific case, profiles of these two functions were plotted for immediate perusal by using a plotting subroutine. Computational times ran from fractions of a minute to 30 minutes.

RESULTS AND DISCUSSION

General Solutions

The difference solutions are presented in the form of nondimensionalized curves so that these results can be applied over a range of operating conditions, tube geometry, and material properties. In figure 2, the dimensionless temperature φ of the inner radius surface through which the heat was removed from the storage material is plotted against the dimensionless time τ for a range of dimensionless heats of fusion F. These surface-temperature - time plots are presented for various values of R_o, which is the nondimensional radius of the heat-transfer surface. In figure 3, the dimensionless thickness of solidification L of the storage material is plotted against the dimensionless time τ for several values of dimensionless heat of fusion and dimensionless radius.

Utilization of figures 2 and 3 necessitates the choice of a storage material along with the knowledge of the material fusion temperature, heat of fusion, thermal conductivity, density, and specific heat. In addition, the cooling or dark time, the overall heat-transfer coefficient, and the heat-transfer surface radius must be specified. To obtain the storage-material surface temperature at the end of a specified dark time, the time τ must be calculated from the orbit dark time, the overall heat-transfer coefficient, and the material properties. The heat of fusion F is then calculated from the thermal properties of the heat-storage material and the local bulk temperature. The radius R_o is calculated from the inner radius, the overall heat-transfer coefficient, and the thermal conductivity. The value of radius R_o calculated from these quantities probably will not correspond to the values of the plots presented in this report; therefore, interpolation may be necessary. When the values of dimensionless time and heat of fusion are known, the proper R_o plot may be entered and the temperature φ obtained. The absolute sur-

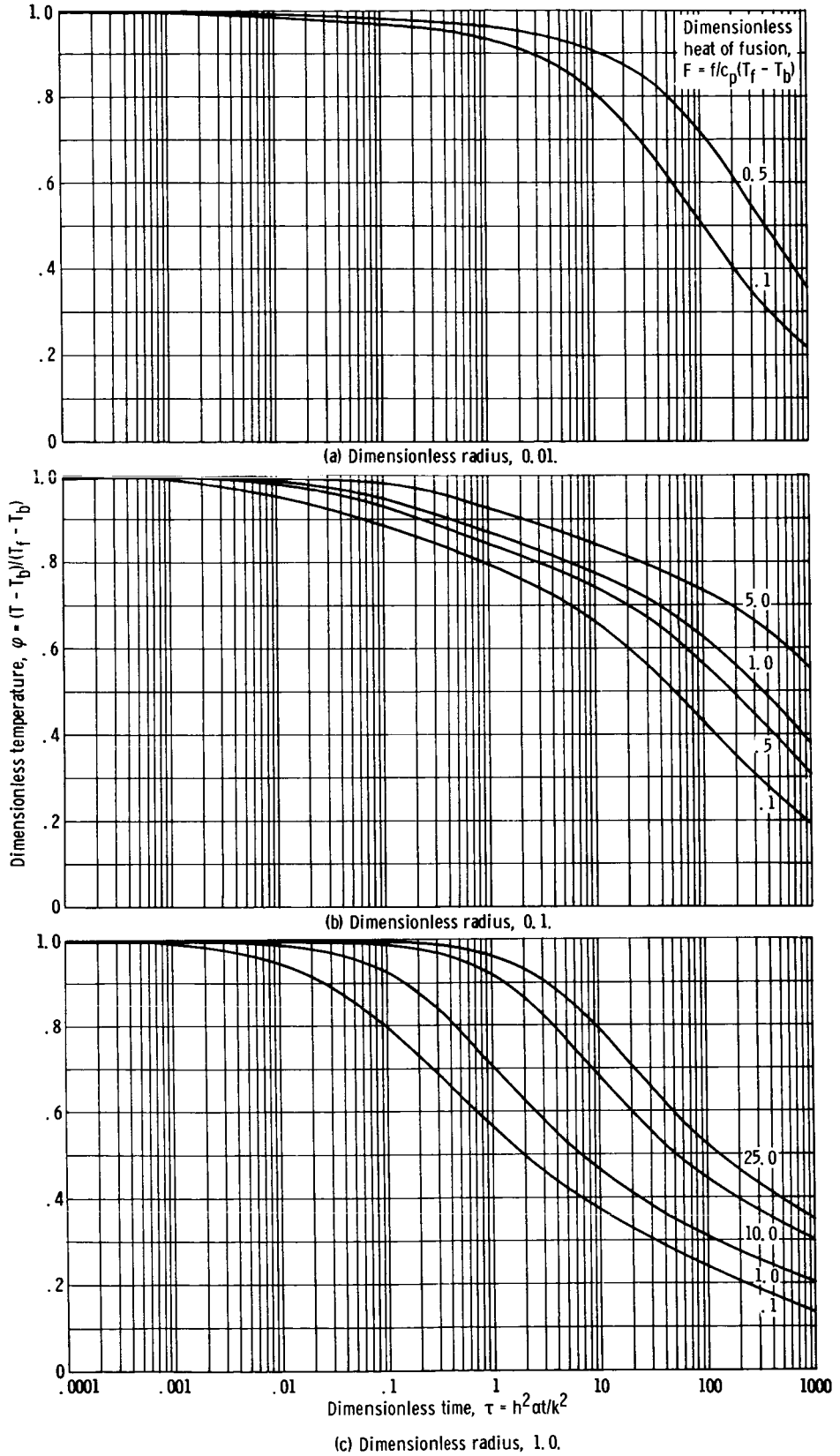

Figure 2. - Time-temperature relations for various dimensionless heats of fusion.

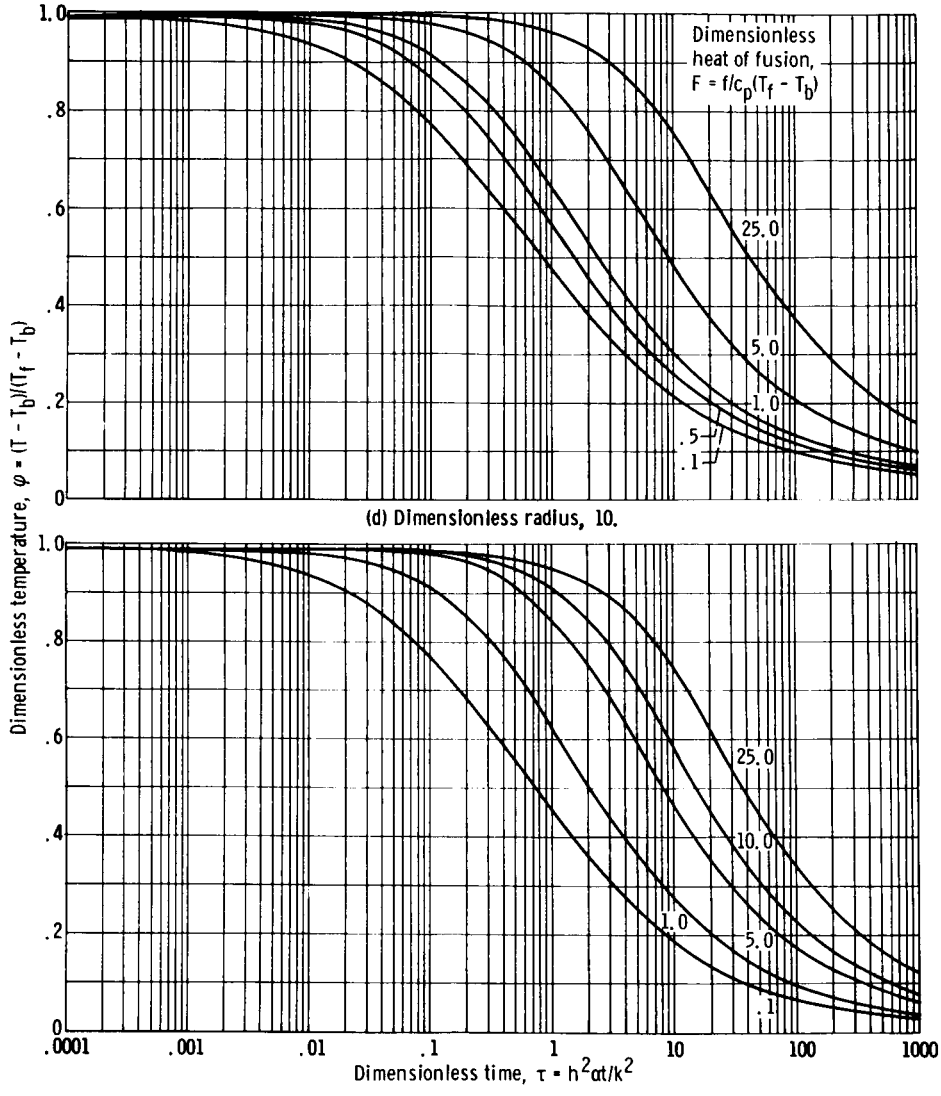

(d) Dimensionless radius, 10.

(e) Dimensionless radius, 100.

Figure 2. - Concluded.

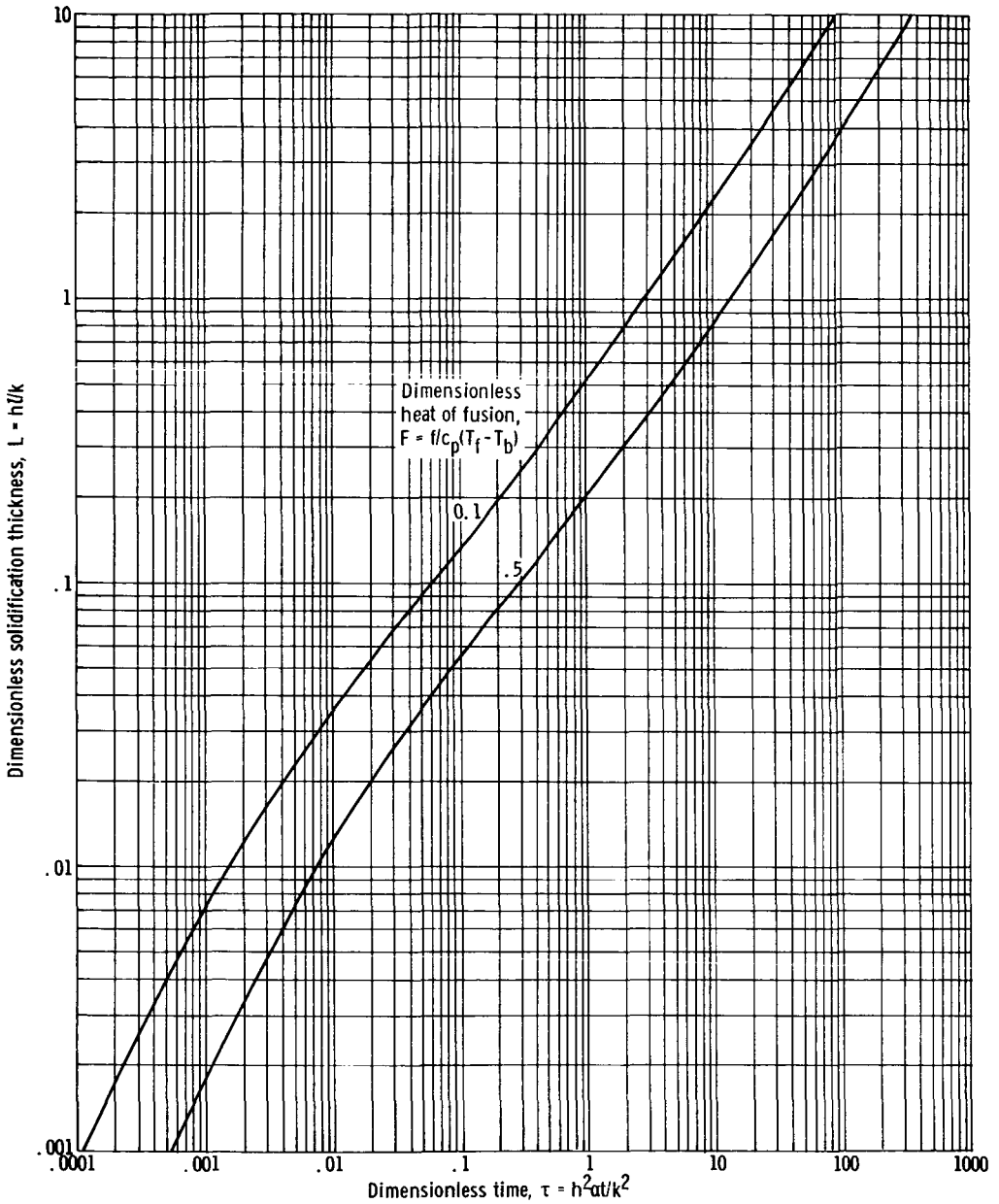

(a) Dimensionless radius, 0.01.

Figure 3. - Time - solidification-thickness relations for various dimensionless heats of fusion.

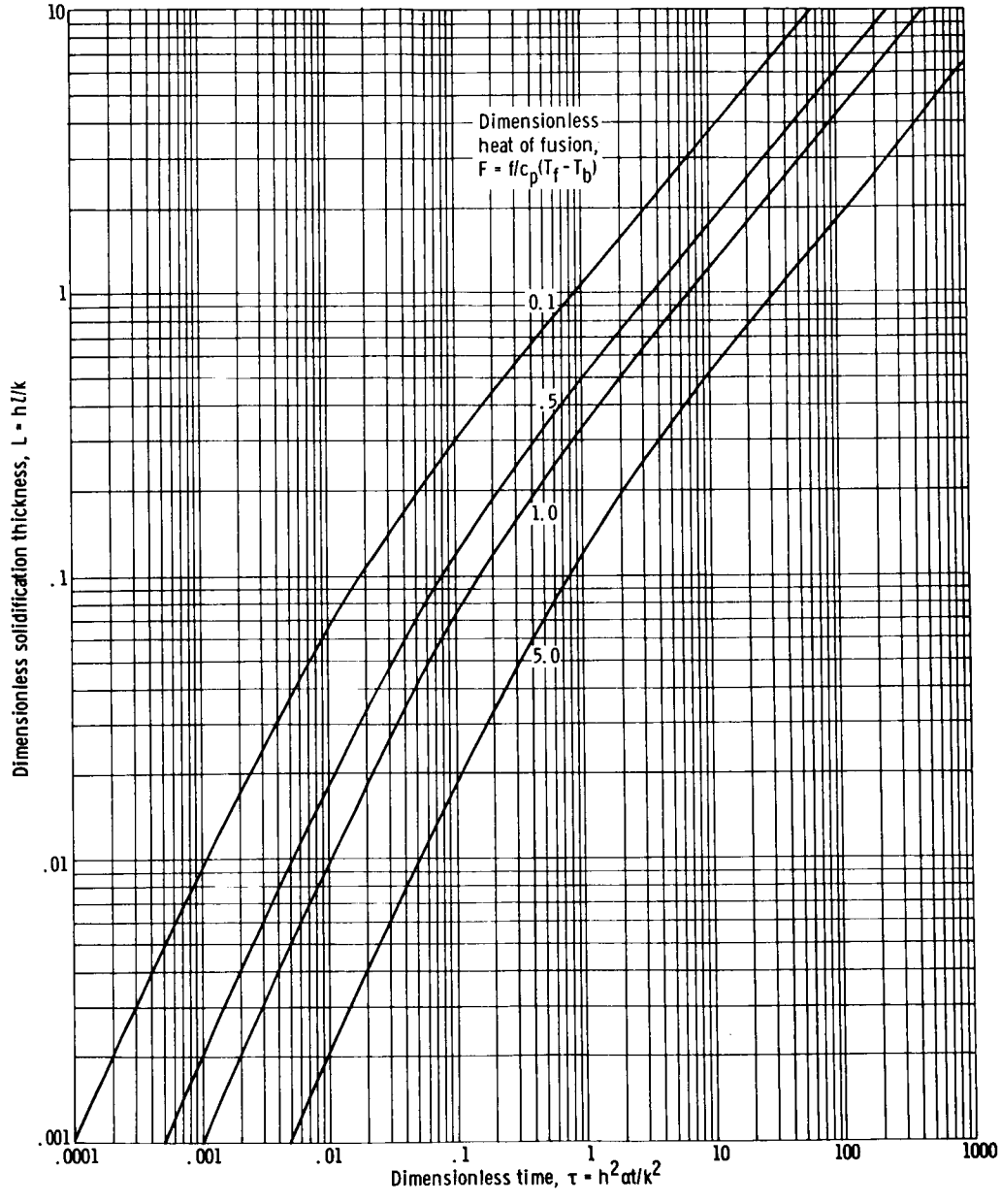

(b) Dimensionless radius, 0.1.

Figure 3. - Continued.

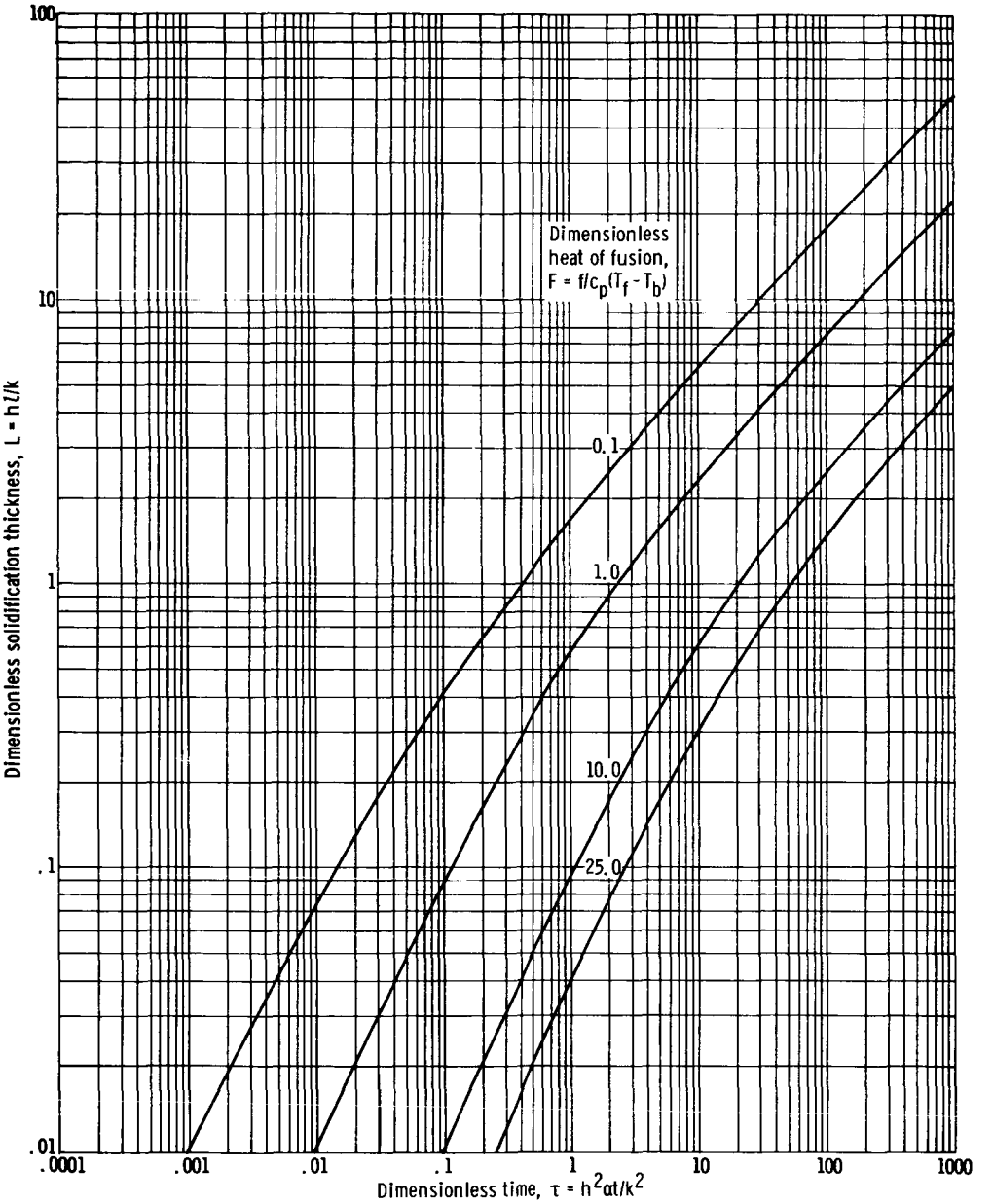

(c) Dimensionless radius, 1.0.

Figure 3. - Continued.

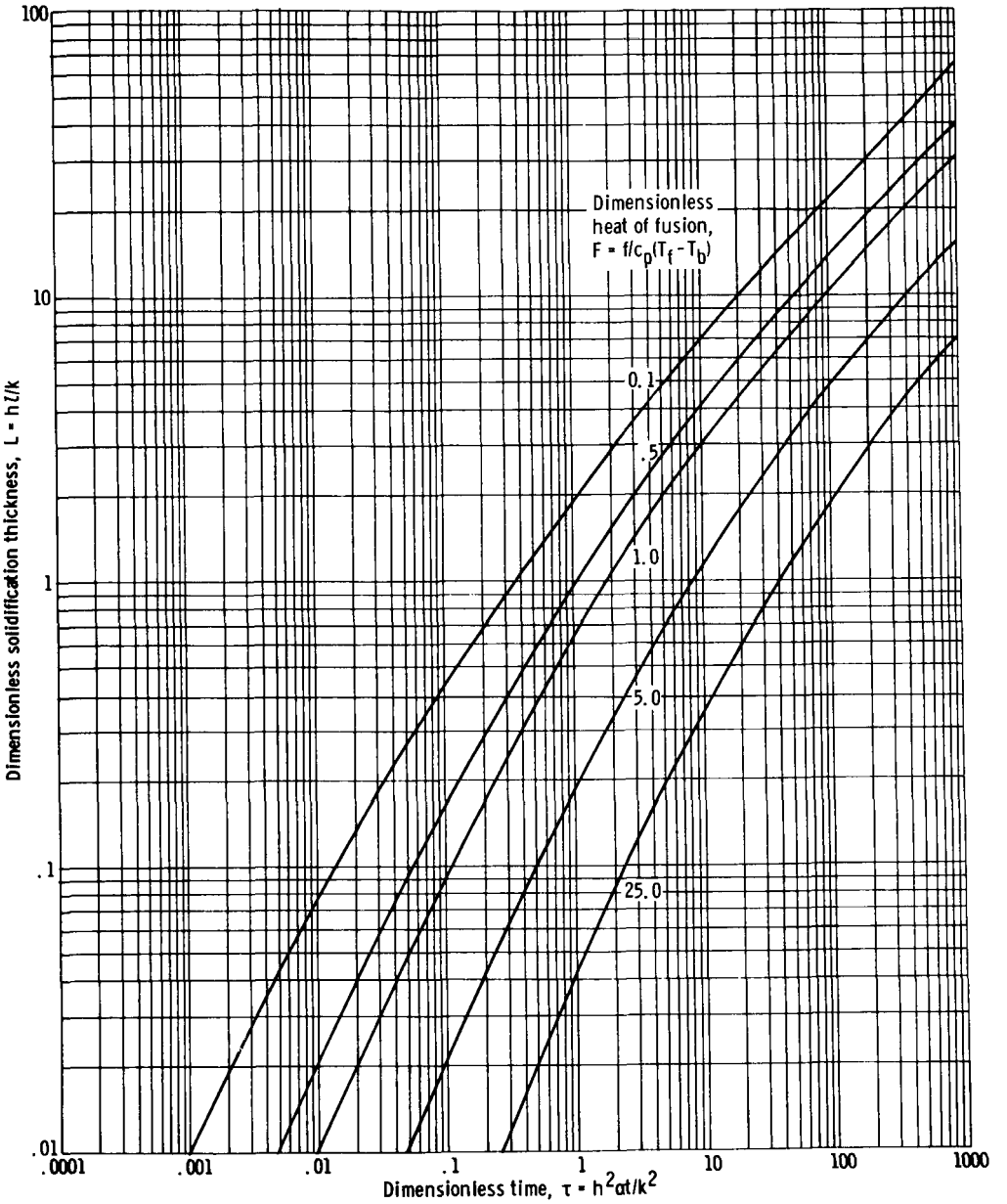

(d) Dimensionless radius, 10.0.

Figure 3. - Continued.

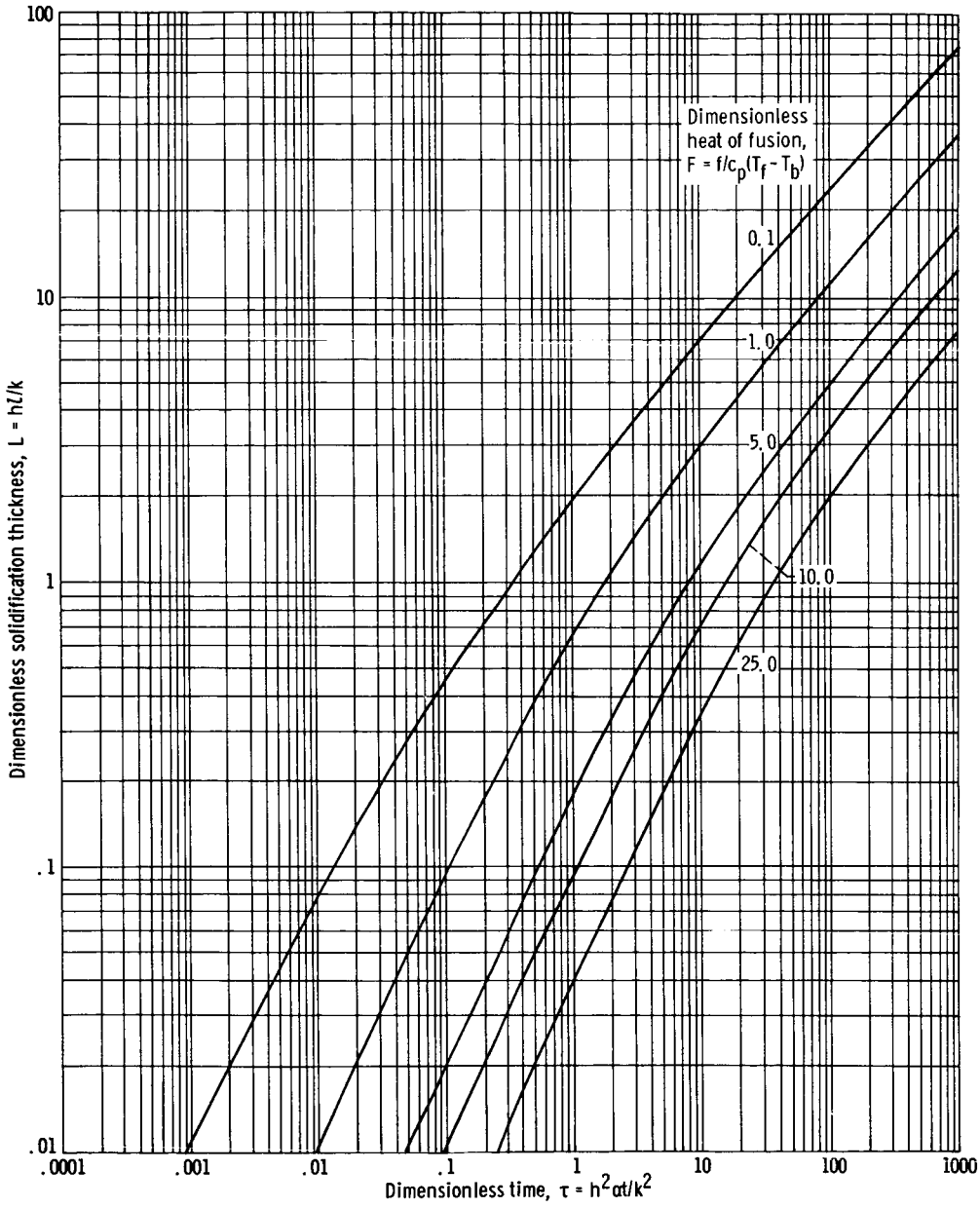

(e) Dimensionless radius, 100.0.

Figure 3. - Concluded.

face temperature at the end of the specified cooling time is then obtained from the definition of φ and from the material fusion and fluid bulk temperatures. The solutions for dimensionless thickness of solidification (fig. 3) are obtained in a similar manner and are dimensionalized with the proper parameters. The nondimensional solutions presented in this report can be applied to a wide range of axisymmetric solidification problems, such as metal casting and ice formation.

Comparison of axisymmetric and one-dimensional solutions. - The variation of dimensionless temperature with dimensionless time for several values of radius at a given value of heat of fusion is shown in figure 4. For low values of time the surface-temperature ratio remains relatively high and does not vary appreciably with radius or from axisymmetric to one-dimensional solutions (ref. 1). As the time increases, variation of the temperature ratio with radius becomes significant. At a given time and for a given initial heat-rejection rate the configuration with a low value of inner surface radius exhibits a higher temperature ratio. This effect occurs because the ratio of frozen storage material volume to heat-transfer surface area is higher for the low values of dimensionless radius and the result is a lower solidification thickness and therefore a lower temperature drop from the fusion interface to the inner radius surface. As the value of radius increases, the surface temperature ratio decreases, until at a value of dimensionless radius of 100 the axisymmetric and the one-dimensional geometries are similar and the solutions correspond. The slight divergence of the comparable axisymmetric and one-dimensional cases can be attributed to the differing methods of solution and to cumulative error. It is observed that, for longer dark times and for values of dimensionless radius less than approximately 100, the one-dimensional solutions fail to depict accurately the true temperature history, and therefore the axisymmetric solutions should be

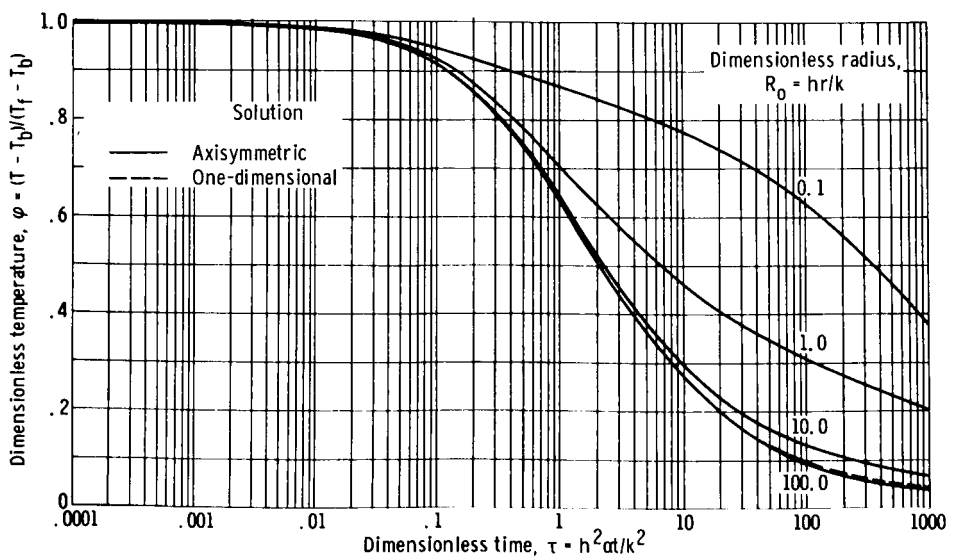

Figure 4. - Comparison of axisymmetric time-temperature relations for various dimensionless radii with one-dimensional relations. Dimensionless heat of fusion, 1.0.

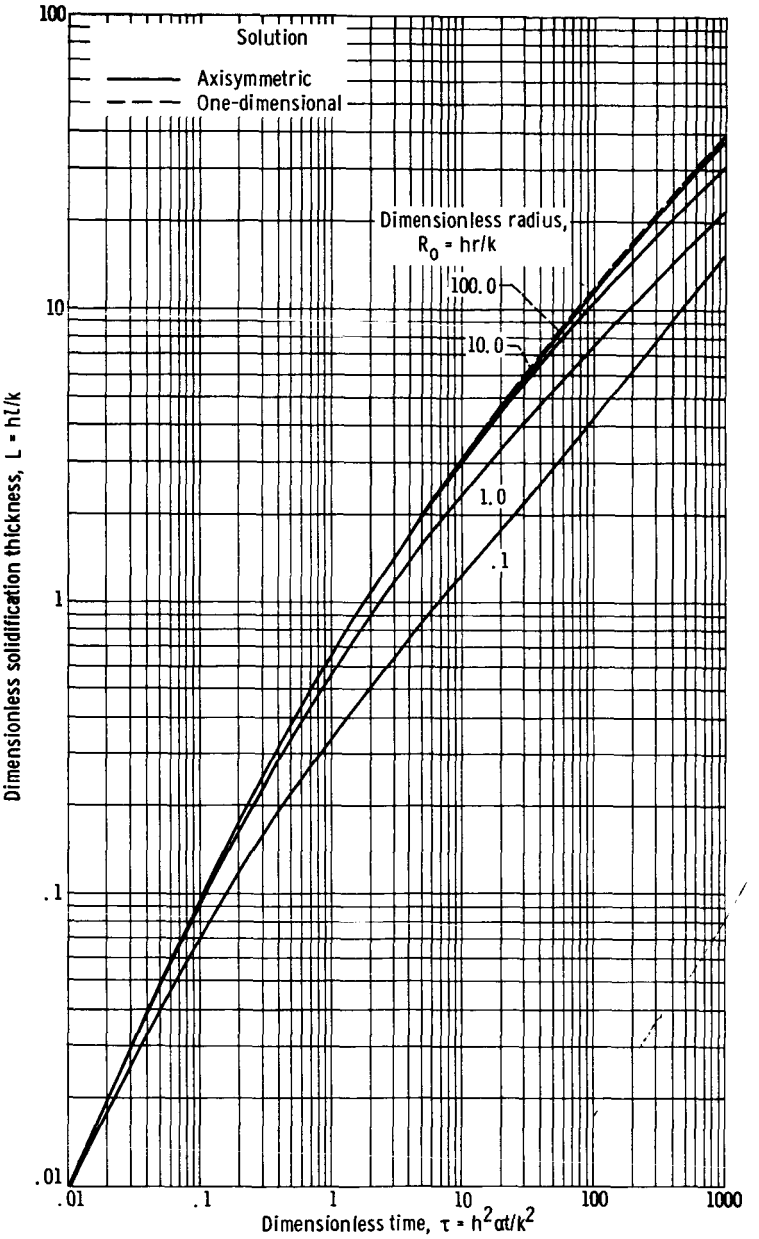

Figure 5. - Comparison of axisymmetric time - solidification-thickness relations for various dimensionless radii with one-dimensional relations. Dimensionless heat of fusion, 1.0.

used in these cases. These comments are also relevant to figure 5, which compares the solidification thickness for several axisymmetric cases with a one-dimensional solution. Thus, utilization of one-dimensional solutions for low radii can result in an inefficient overdesign of the thermal-energy-storage system.

Analysis of parametric relations. - The relation between the heat-rejection rate, cooling time, and heat-transfer surface radius and the dependent parameters, surface temperature and solidification thickness, can be qualitatively established from figures 4 and 5. It is assumed that the heat-rejection rate can be expressed as $q = h(T - T_b)$ for a constant bulk temperature. Then from equation (3) in the section ANALYSIS it can be observed that the dimensionless time parameter increases with the second power of the heat-transfer coefficient. In addition, an increase in the heat-transfer coefficient increases the dimensionless radius parameter linearly. The combined effect of an increase in these two parameters, due to an increase in the heat-transfer rate, is an augmented drop in the surface temperature ratio. The cooling time and the surface radius affect their respective dimensionless parameters linearly. Therefore, for the cases considered here the surface temperature is more sensitive to changes in heat-rejection rate than to changes in either cooling time or heat-transfer surface radius.

The dimensionless solidification thickness shown in figure 5 increases at a given time as the dimensionless radius increases. The low value of radius exhibits a lower solidification thickness because the ratio of frozen storage material volume to heat-transfer surface area is higher for low values of radius. Thus, a low radius configuration can provide the same initial thermal energy flux with a lower solidification thickness because of the axisymmetric geometry. As the dimensionless radius increases, the axisymmetric solutions approach the one-dimensional solution of reference 1. The difference between the solutions diminishes at the lower values of time. An analysis similar to that made for figure 4 shows that over the range of parameters studied the solidification thickness is most sensitive to changes in cooling time.

System Analysis

The general solutions of figures 2 and 3 are used to analyze the performance of a family of cavity-absorbers in terms of surface temperature and solidification thickness. The cavity-absorber component of a space auxiliary-power system receives the incident solar radiation during the sunlit portion of the orbit. The absorbed solar radiation melts the thermal-energy-storage material contained between the cavity wall and the tube wall of the loop. This melting transfers heat to the energy-conversion device. When the solar collector of the space vehicle is not receiving radiation from the Sun, the storage material will solidify and thereby provide thermal energy from its heat of fusion to the

energy-conversion system.

Axially constant heat-flux thermal-storage system. - The thermal characteristics of a family of storage systems using lithium hydride storage material are investigated in figure 6. Lithium hydride properties listed in table I were obtained from references 5 and 6. A dark time or total cooling time of 35 minutes was specified. Solutions were obtained by using figure 2 for a range of initial heat-rejection rates and for three tube radii. An infinite tube wall conductivity and a constant bulk temperature were assumed for the results presented in figure 6. This design approach can be referred to as the constant-heat-flux solution because a calculation is performed at a given axial station and then applied along the length of the heat-transfer tube. This solution is a good approximation when the total enthalpy rise of the heat-transfer fluid is not excessive and the heat-transfer rates are relatively low. As expected, the surface temperature at the end of the dark time decreased as the initial heat-rejection rate increased. The various tube radii show the effect of the ratio of the storage material volume to the tube heat-transfer surface area in the efficient utilization of the thermal-storage material. The lowest radius tube considered (fig. 6) is apparently most efficient because for a given heat-rejection rate it displays the highest surface temperature.

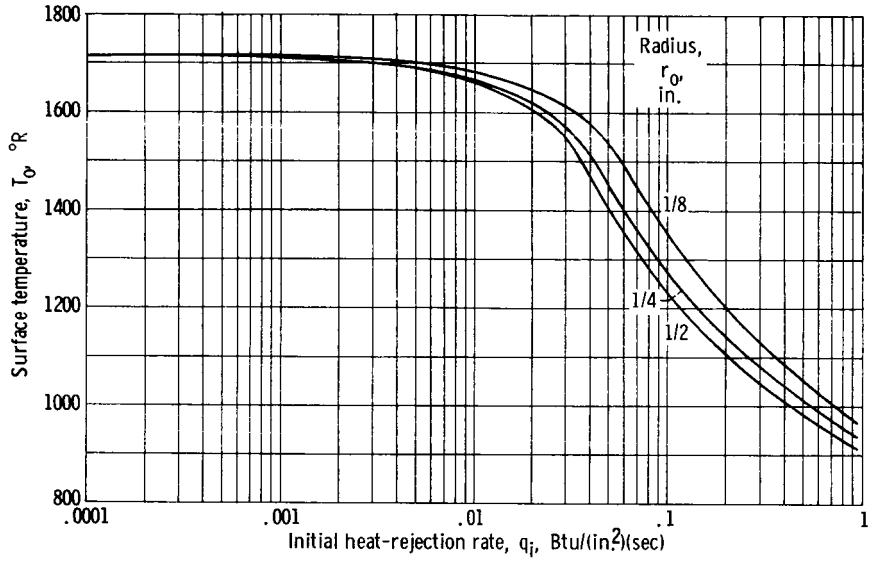

Figure 6. - Lithium hydride storage-material surface temperature as function of initial heat-rejection rate for various radii. Dark time, 35 minutes.

TABLE I. - PROPERTIES OF LITHIUM HYDRIDE

Fusion temperature, T_f, °R	1715
Heat of fusion, f, Btu/lb	1251
Thermal conductivity, k, Btu/(hr)(ft)(°R)	2.4
Density, ρ, lb/ft^3	43
Specific heat, c_p, Btu/(lb)(°R)	1.9

Figure 6 can be used to determine the limiting heat flux available from a thermal-storage system. For example, if the cavity-absorber outlet temperature required at the

end of the 35-minute dark time is 1500° R, the maximum initial heat-rejection rate available from a storage system with 1/8-inch-radius tubes is 0.058 Btu per square inch per second. The storage system must then be designed within this heat flux limit but with sufficient tube heat-transfer surface area to provide the required enthalpy rise to the heat-transfer medium during the dark period of the orbit. In addition, the heat-transfer surface area must be increased because the heat-rejection rate is not constant over the dark period. If the heat flux is characterized by $q = h \Delta T$, then, for a constant heat-transfer coefficient, the heat flux at the end of the dark time will be the initial rate corrected by the ratio of the final to the initial temperature difference. In this example the final heat flux will be 0.043 Btu per square inch per second. Therefore, to supply the total thermal energy required during the dark time, the surface area, and hence the tube length, must be increased by approximately 35 percent to compensate for this decrease in heat-transfer rate.

For a given dark time, figure 6 indicates that a tube radius which provides a high ratio of storage-material volume to tube surface area most efficiently utilizes the storage material. However, this factor is limited, depending on the heat-transfer medium flowing in the tube, because the pressure drop may become appreciable as the tube radius is decreased. From a system-weight standpoint the optimum tube configuration will also be affected by the ratio of the tube wall material density to the storage material density.

To complete a design study, a knowledge of the solidification thickness is required. The solidification depths for the family of lithium hydride thermal-energy systems described previously are presented in figure 7. Solidification thicknesses were obtained by using figure 3 for a range of initial heat-rejection rates. The thicknesses increased as the heat flux and the tube radius increased. For the example of a system with 1/8-inch-

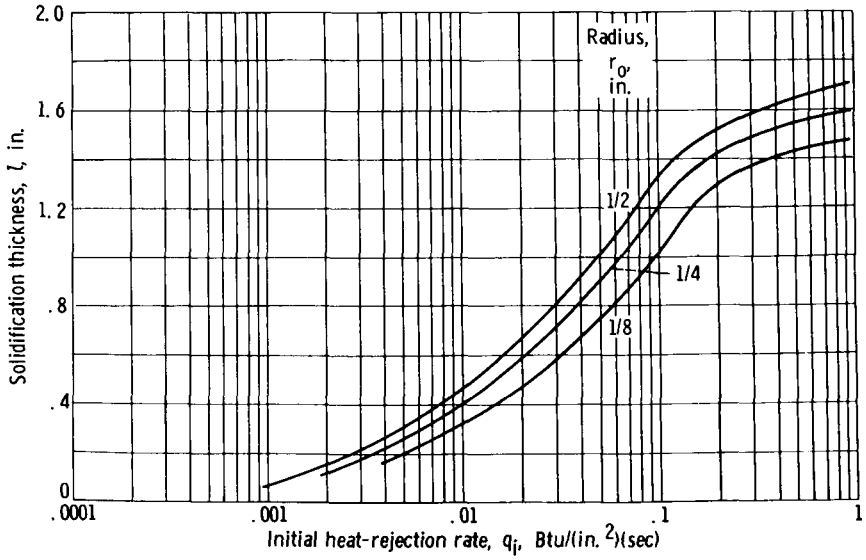

Figure 7. - Lithium hydride storage-material solidification thickness as function of initial heat-rejection rate for various radii. Dark time, 35 minutes.

radius tubes, at a heat flux of 0.058 Btu per square inch per second. The solidification thickness is approximately 0.80 inch. The heat-transfer surface area and therefore the total tube length are obtained from the required enthalpy rise of the heat-transfer medium. With the total tube length and the solidification depth, the volume and weight of the thermal-energy storage material can be calculated.

Axially varying heat-flux thermal-storage system. - When the thermal-storage system requirements specify a relatively high total enthalpy rise or a high heat-rejection rate, a more exact calculation may be needed for design purposes. The more exact solution may be desired to analyze the system because of the axially variable system parameters which control the heat-transfer process. As the heat-transfer medium flows down the tube, its bulk temperature is raised by heat addition from the tube wall. To supply the thermal energy, the heat-storage material solidifies and causes the outer radius wall temperature to decrease so that the wall temperature varies along the tube in the axial direction. Therefore, the sink temperature and the source temperature vary along the tube axis.

The axisymmetric solutions of figure 2 were applied to the axially variable heat-flux case by dividing the tube into finite axial increments and assuming properties and parameters as constant over these small increments. As an example, a system composed of lithium hydride storage material, mercury heat-transfer fluid, and a stainless steel tube with an outer radius of 1/8 inch and a wall thickness of 0.030 inch was considered. The liquid mercury was assumed to enter the thermal-storage component at 860° R and to have a flow velocity of 2 feet per second. Prior to the entrance of the mercury the tube outer radius wall temperature is axially uniform at the storage-material fusion temperature. As the mercury flows down the tube, heat transfer occurs from the hot tube to the cooler fluid. At a given axial location the heat transfer proceeds at a decreasing rate as the wall temperature approaches the local mercury bulk temperature. Thus, the heat transfer from the storage material to the fluid can be described approximately as a temperature wave which travels along the tube axis. If the traveling temperature wave is observed from a fixed tube axial location, the temperature histories shown in figure 8 are obtained. The temperatures of the wall on the lithium hydride side and on the mercury side are presented, as well as the mercury bulk temperature. These respective temperatures are presented at two tube axial locations. At a given axial position, the heat-transfer cycle is assumed to begin when the heat-transfer medium reaches that station. The period of time that heat is transferred at a given axial location is defined as the heat-transfer cycle time. Because of the likeness to a wave phenomenon, the temperature histories at different axial positions may be plotted against the cycle time for comparison. The outer radius temperature decreases from the storage-material fusion temperature to the fluid bulk temperature during the heat-transfer cycle at a given axial location. Because of the finite thermal conductivity of the wall material, there is a

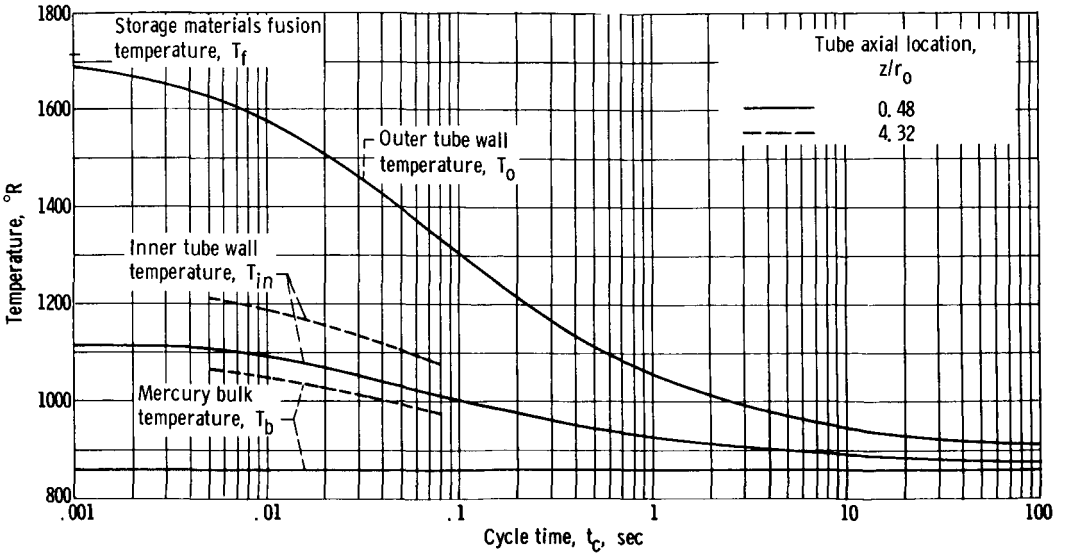

Figure 8. - Outer and inner tube wall temperature and mercury bulk temperature as functions of cycle time at two tube axial locations. Storage material, lithium hydride; heat-transfer fluid, liquid mercury; tube material, stainless steel; tube outer radius, 1/8 inch; tube wall thickness, 0.030 inch; heat-transfer coefficient, 0.00676 Btu per square inch per second per °R.

temperature drop through the wall, as indicated by the difference between the outer and inner radius wall temperature. The difference between the respective inner radius wall temperatures and the fluid bulk temperature curves is an indication of the instantaneous heat-transfer rate for the assumption of a constant heat-transfer coefficient. The heat-transfer rate is a maximum at the beginning of a cycle and then decreases as time approaches zero at a given axial location.

As the mercury flows along the tube, its temperature is raised by the addition of heat from the solidifying lithium hydride, as shown by the dashed bulk-temperature curve in figure 8. The inner radius wall temperature also assumes a higher level at the station farther downstream. The instantaneous heat-transfer rate at the downstream axial station decreases from the value at the tube entrance, as indicated by the decreased difference between the wall and bulk temperatures. The outer radius temperature-time plot is shown to be the same at the two axial stations considered in figure 8 because the heat-transfer coefficient and the dimensionless heat of fusion are assumed to be axially constant. The effect of changing the bulk temperature in the dimensionless heat of fusion would be to raise the outer radius temperature a maximum of 3.8 percent at the downstream location. This effect was ignored in figure 8. However, for some designs the effect of varying the bulk temperature on outer radius temperature could be significant and therefore should be considered in those cases. It can be observed from figure 8 that the difference between the wall and bulk temperatures, which is an indication of the instantaneous heat-transfer rate, decreases with time at a given axial location and also decreases at a given cycle time with distance down the tube.

To complete a design study of an axially varying heat-flux storage system, the instantaneous heat-transfer rate must be integrated over the cycle time at each axial tube increment. The integrated heat-transfer rate at a given axial position multiplied by the incremental tube-surface area indicates the amount of thermal energy absorbed by the heat-transfer fluid at that axial location. These calculations must be repeated at a number of axial stations until the total thermal energy required during the dark time is obtained. When this heat balance is made, the axial length of the tube is known. The solidification thickness can be obtained from figure 3. The volume and weight of the storage material can then be calculated by using the required tube length and solidification thickness.

CONCLUDING REMARKS

This analysis considered a transient-heat-conduction problem with a phase change in the axisymmetric conducting medium and heat transfer at the inner radius only. Nondimensional finite-difference solutions for surface temperature and solidification thickness were obtained for a range of cooling time, initial heat-rejection rate, tube diameter, and storage-material properties. The storage material was assumed to be initially at the fusion temperature, and the material properties were assumed constant with temperature. The nondimensional solutions presented in this report can be applied to a wide range of axisymmetric solidification problems, such as metal casting and ice formation.

Analysis of these general solutions, as applied to the thermal-energy-storage component of a direct-energy-conversion system, indicates that (1) utilization of axisymmetric solutions is recommended for low radii or long cooling times to prevent inefficient overdesign of the thermal-energy-storage system; (2) the surface temperature of the storage material is more sensitive to changes in heat-rejection rate than changes in either cooling time or heat-transfer surface radius; and (3) the solidification thickness is more a function of cooling time than of heat-rejection rate or surface radius.

Lewis Research Center,
National Aeronautics and Space Administration,
Cleveland, Ohio, September 15, 1966,
129-01-09-08-22.

APPENDIX - SYMBOLS

c_p specific heat, Btu/(lb)(^{o}R)

F dimensionless heat of fusion, $f/c_p(T_f - T_b)$

f heat of fusion, Btu/lb

h heat-transfer coefficient, Btu/(in.^{2})(sec)(^{o}R)

k thermal conductivity, Btu/(hr)(ft)(^{o}R)

L dimensionless solidification thickness, $h\ell/k$

ℓ solidification thickness, in.

q heat-rejection rate, Btu/(in.^{2})(sec)

R dimensionless radius, hr/k

r radius, in.

T temperature, ^{o}R

t time, sec

z axial distance, in.

α thermal diffusivity, ft^2/hr

ρ density, lb/ft^3

τ dimensionless time, $h^2\alpha t/k^2$

φ dimensionless temperature, $(T - T_b)/(T_f - T_b)$

Subscripts:

b bulk

c cycle

f fusion

i initial

in inside wall

o outside wall

REFERENCES

1. Cullom, Richard R.; Robbins, William H.; and Todd, Carroll A.: One-Dimensional Heat-Transfer Analysis of Thermal-Energy Storage for Solar Direct-Energy-Conversion Systems. NASA TN D-2119, 1964.

2. Siegel, Robert; Savino, Joseph M.: An Analysis of the Transient Solidification of a Flowing Warm Liquid on a Convectively Cooled Wall. Paper presented at the 3rd International Heat Transfer Conference, Chicago, Illinois, Aug. 8-12, 1966. (Also available as NASA TM X-52176.)

3. Hrycak, Peter: Problem of Solidification with Newton's Cooling at the Surface. AIChE J., vol. 9, no. 5, Sept. 1963, pp. 585-589.

4. Crank, J.; and Nicolson, P.: A Practical Method for Numerical Evaluation of Solutions of Partial Differential Equations of the Heat-Conduction Type. Cambridge Phil. Soc. Proc., vol. 43, pt. 1, Jan. 1947, pp. 50-67.

5. Hodgman, Charles D., ed.: Handbook of Chemistry and Physics. Thirty-eighth ed., Chem. Rubber Pub. Co., 1956-1957.

6. Wolfe, G. W.; and Arne, V. L.: Thermal Properties of Solids. Rep. no. AST-E9R-12073, Chance Vought Aircraft, Inc., Sept. 1, 1959.

"The aeronautical and space activities of the United States shall be conducted so as to contribute . . . to the expansion of human knowledge of phenomena in the atmosphere and space. The Administration shall provide for the widest practicable and appropriate dissemination of information concerning its activities and the results thereof."

—NATIONAL AERONAUTICS AND SPACE ACT OF 1958

NASA SCIENTIFIC AND TECHNICAL PUBLICATIONS

TECHNICAL REPORTS: Scientific and technical information considered important, complete, and a lasting contribution to existing knowledge.

TECHNICAL NOTES: Information less broad in scope but nevertheless of importance as a contribution to existing knowledge.

TECHNICAL MEMORANDUMS: Information receiving limited distribution because of preliminary data, security classification, or other reasons.

CONTRACTOR REPORTS: Technical information generated in connection with a NASA contract or grant and released under NASA auspices.

TECHNICAL TRANSLATIONS: Information published in a foreign language considered to merit NASA distribution in English.

TECHNICAL REPRINTS: Information derived from NASA activities and initially published in the form of journal articles.

SPECIAL PUBLICATIONS: Information derived from or of value to NASA activities but not necessarily reporting the results of individual NASA-programmed scientific efforts. Publications include conference proceedings, monographs, data compilations, handbooks, sourcebooks, and special bibliographies.

Details on the availability of these publications may be obtained from:

SCIENTIFIC AND TECHNICAL INFORMATION DIVISION

NATIONAL AERONAUTICS AND SPACE ADMINISTRATION

Washington, D.C. 20546